

Dynamic impact of the COVID-19 lockdown intervention policies on network structure of energy futures return connectedness

Baifan Chen^a, Jionghao Huang^c, Xintong Zhu^a, Xiaohua Xia^{a,b,*}

^a School of Applied Economics, Renmin University of China, Beijing, China

^b Institute of China's Economic Reform and Development, Renmin University of China, Beijing, China

^c School of Economics, Peking University, Beijing, China

ARTICLE INFO

Handling Editor: Panos Seferlis

JEL classification:

C58
G10
Q02

Keywords:

COVID-19 lockdown
TVP-VAR frequency connectedness
Directed multi-layer dynamic connectedness network
Policy change point

ABSTRACT

This work investigates the dynamic impact of COVID-19 lockdown policies, implemented to curb the pandemic's spread, on the structure of the energy futures return connectedness network (EFRCN). Firstly, we measured the connectedness of 20 energy futures return series using the time-varying parameter vector autoregression (TVP-VAR) frequency connectedness approach and constructed a directed multi-layer dynamic EFRCN. Secondly, we developed a novel statistical indicator, the ratio of average vertex out-strength to average vertex in-strength, to represent the spillover intensity of a specific network layer. Finally, we utilized the pruned exact linear time (PELT) algorithm to pinpoint structural change points of COVID-19 lockdown policies and explored the change in the EFRCN structure before and after these change points. The empirical findings demonstrate that the scales of population and gross domestic product (GDP) impacted by the COVID-19 lockdown positively drive the average vertex strength, density, and clustering coefficient of the EFRCN, as well as the return spillover intensity of oil and power futures markets, respectively. Conversely, the regression results exhibit noteworthy negative causal relationships between the scales of population and GDP impacted by the COVID-19 lockdown and the return spillover intensity of coal and natural gas futures markets for non-periodic and short-term networks. Furthermore, the empirical results illustrate distinct structural changes in the evolution of global indicators of the non-periodic and short-term networks at the change points of COVID-19 lockdown policies before June 2020. To sum up, COVID-19 lockdown intensification increases the clustering of the EFRCN and significantly enhances the net spillover effects of oil and power futures markets within the EFRCN. Moreover, the changes in COVID-19 lockdown policies significantly influence the EFRCN's structure.

1. Introduction

The COVID-19 pandemic, which emerged in early 2020, rapidly spread worldwide, imposing substantial hazards on the global population's health, well-being, and economic development. According to data disclosed by the World Health Organization, as of May 10, 2023, the cumulative number of confirmed COVID-19 cases globally reached 765,903,278, with a reported cumulative death toll of 6,927,378. Economically, the "World Economic Outlook" report, issued by the International Monetary Fund (IMF) in October 2021, indicates a global economic downturn of 3.1% in 2020 compared to the preceding year. Developed economies experienced a decline of 4.5%, while emerging markets and developing economies encountered a decline of 2.1%.

In order to safeguard public health and mitigate the impact of the

COVID-19 pandemic on the economy and society, countries vigorously enforced lockdown measures during the early stages of the outbreak when an effective vaccine had not yet been successfully developed. The implementation of lockdown policies has come with a reduction in social interactions. Simultaneously, it has substantially increased homebound time and online working hours, decreased travel frequency, and shortened travel distances. Although such measures effectively severed the transmission chain of the virus, they also incurred additional intervention costs. For instance, suicide rates increased (Ruiz Sánchez, 2021), psychological anxiety rose (Wu et al., 2021), financial market panic ensued (Umar and Gubareva, 2020), mass layoffs occurred (Bartik et al., 2020), poverty exacerbated (Tchouamou Njaya, 2023), food crises emerged (Clapp and Moseley, 2020), and supply chain disruptions unfolded (Chen et al., 2021), among other consequences.

* Corresponding author. No. 59 Zhongguancun St., Haidian District, Beijing, 100872, China.

E-mail address: xiaxh.email@gmail.com (X. Xia).

<https://doi.org/10.1016/j.jclepro.2023.139802>

Received 4 June 2023; Received in revised form 8 November 2023; Accepted 16 November 2023

Available online 21 November 2023

0959-6526/© 2023 Elsevier Ltd. All rights reserved.

Since the outbreak of COVID-19, there has been a rapid increase in literature exploring the economic impacts of the COVID-19 pandemic and intervention measures. Some studies assessed the losses in macroeconomic output attributable to implementing lockdown interventions to mitigate the spread of COVID-19 (Behera et al., 2021). Wu et al. (2023) systematically evaluated the adverse effects of China's lockdown interventions on its economy. The counterfactual analysis conducted by Ke and Hsiao (2022) revealed that the lockdowns implemented in Hubei province, China, resulted in a 37% GDP loss in Q1 2020. Fezzi and Fanghella (2020) utilized power data to estimate that Italy's most stringent three-week lockdown precipitated a 30% decline in its GDP. Coccia (2021) noted that prolonged societal lockdowns engendered systemic economic deterioration. Relatedly, Adams-Prassl et al. (2020) examined the detrimental effects of COVID-19 and lockdown policies on the labor market. Forsythe et al. (2020) employed real-time online job vacancy data from the U.S., revealing a decline in recruitment across all industries as a result of lockdown interventions. In parallel, some scholars investigated the impact of COVID-19 and lockdown interventions on consumer behavior (Goolsbee and Syverson, 2021) and established virtual scenario simulations to assess the macroeconomic performance under different intervention scenarios (McKibbin and Fernando, 2021). Furthermore, others explored the impact of COVID-19 and its interventions on financial markets (Shehzad et al., 2021). For example, Shehzad et al. (2020) observed a negative impact of COVID-19 on stock markets, whereas Bouri et al. (2022) discovered that lockdowns had a positive effect on industry stock return.

The growing body of literature is exploring the impact of COVID-19 on the internal or cross-market linkages of asset return or volatility in financial assets and commodities markets (Huang et al., 2023). Within these studies, a strand of the literature delves into the cross-asset or internal connectedness of return or volatility for a single market. For example, Dong et al. (2022) studied the impact of the COVID-19 pandemic on the connectedness of volatility within global stock sectors. Similarly, Akyildirim et al. (2022) examined the effects of the COVID-19 pandemic on the connectedness of return within the global energy markets. Another strand of the literature investigates the change in the connectedness of return or volatility across multiple markets during the COVID-19 pandemic (Farid et al., 2022). This strand of research predominantly focused on two directions. First, it investigates the effects of the COVID-19 pandemic on the connectedness between financial and energy commodity markets (Mensi et al., 2023). Second, it explores the impact of the COVID-19 pandemic on the connectedness of return or volatility between energy and non-energy commodities (Cui and Maghyreh, 2023). Other scholars analyzed the changes in the connectedness of return or volatility between gold and cryptocurrencies (González et al., 2021), Bitcoin and crypto assets (Katsiampa et al., 2022), carbon emission trading and commodity markets (Qi et al., 2023), as well as carbon markets and Non-fungible tokens (NFTs) (Liu, 2023). Mainstream research converged on a consensus that during the COVID-19 pandemic, both the internal and cross-market linkages of return or volatility in financial and commodities markets have experienced a significant increase (Mishra et al., 2023).

A limited body of literature has analyzed the changes in the dependency structure of return and risk among financial or commodity assets during the COVID-19 pandemic. For instance, Ouyang et al. (2022) identified a reversal in the role of some bulk commodities within the risk transmission network after the outbreak of the COVID-19 pandemic. Bouri et al. (2021) found that the structure of return connectedness among gold, crude oil, global stocks, currencies, and bonds remained relatively stable before the pandemic outbreak but experienced significant changes after the emergence of the COVID-19 pandemic. Analogous to these studies, some scholars have observed noteworthy changes in the network topology structure of financial or commodity markets under the shock of COVID-19. For example, So et al. (2021b) found that during the COVID-19 outbreak, the density and clustering coefficient of the network, based on the partial correlation of

financial return, stood at relatively high values. Moreover, So et al. (2021a) used Granger causality tests to confirm that the density of the pandemic network serves as a leading indicator of the financial network. Bahloul and Khemakhem (2021) revealed that early-stage pandemics significantly alter the network structure of return and volatility between commodities and Islamic markets. Similarly, Billio et al. (2021) examined a significant alteration in the network structure after the COVID-19 pandemic. Additionally, Liu and Huang (2022) documented significant changes in the international sovereign risk network under the impact of the COVID-19 shock.

Reviewing related works, we identified two aspects worthy of further investigation within the extant studies. First, most existing literature treats the COVID-19 pandemic as a discrete exogenous event or a unique period and compares the differences in connectedness levels or network topology structure between pre- and post-pandemic periods. There is a lack of consideration of the evolution of the pandemic and the changes in intervention policies when investigating the dynamic connectedness of return and volatility among financial and commodity assets during the pandemic. Second, there is a scarcity of research focusing on the impact of the COVID-19 pandemic and lockdown intervention policies on the network structure of financial or commodity markets. These research focal points constitute the primary objectives of our study.

To bridge this research gap, we focused on investigating the effects of COVID-19 lockdown policies on the structure of the energy futures return connectedness network (EFRCN). Specifically, we are committed to achieving the following research objectives. Firstly, we investigated the relationship between aggregated GDP and populations affected by the COVID-19 lockdown and the structure indicators of the EFRCN. Secondly, we explored the impact of COVID-19 lockdown policies on the spillover effects of return information across different types of energy markets. Finally, we examined how the transformation of global COVID-19 lockdown policies has affected the structure of the EFRCN.

Our study makes three contributions. Firstly, it is the first to investigate the dynamic impact of the COVID-19 lockdown policies on the global energy futures return network structure, thereby extending the existing literature on the impact of the COVID-19 lockdown intervention policies on financial markets. Meanwhile, unlike earlier relevant research that primarily focused on comparing the differences in static connectedness network structures corresponding to the periods before and after the outbreak of COVID-19 (Chen et al., 2022a), we examined the dynamic impact of lockdown policies on the structure of the EFRCN within a continuous sample time interval following the outbreak of COVID-19. Secondly, we applied the average out-strength and in-strength, which are global weighted network indicators, to a multilayer-directed weighted complex network and proposed a new local network structural indicator: the ratio of out-degree to in-degree for a network layer. This new indicator measures the relative strength of information overflow and reception of a specific market in the entire multilayer network system. It lays the study foundation for dynamically identifying changes in the interaction process and strength of information between network layers in different periods. Finally, this paper presents a novel framework for measuring the intensity of the COVID-19 lockdown. The framework aggregates the population and GDP controlled by implementing COVID-19 lockdown policies by integrating the COVID-19 lockdown policies data, administrative boundaries data derived from the Global Administrative Areas Database (GADM), and population distribution information obtained from the LandScan database.

2. Methodology

2.1. Measuring return connectedness

We followed the methodology proposed by Chatziantoniou et al. (2023), which constructs a measurement framework integrating the time-varying parameter connectedness approach (Antonakakis et al.,

2020) and the frequency domain connectedness method (Baruník and Křehlík, 2018). Following the studies of Chatziantoniou et al. (2023), we first briefly introduced the TVP-VAR measure and then the frequency domain.

2.1.1. Time-varying parameter connectedness approach

The time-varying connectedness method developed by Antonakakis et al. (2020) combines the results of Diebold and Yilmaz (2012, 2014) and Koop and Korobilis (2014). This methodology achieves the purpose of dynamically measuring connectedness and overcomes the measurement defects of rolling-window VAR methodology, which include arbitrarily chosen rolling-window size, loss of observations, and outlier-sensitive parameters (Chatziantoniou et al., 2023). The precondition for employing the TVP-VAR-based frequency connectedness methodology is that the utilized variables are stationary. The TVP-VAR (p) model can be written as follows:

$$z_t = \Pi_{1t}z_{t-1} + \Pi_{2t}z_{t-2} + \dots + \Pi_{pt}z_{t-p} + \varepsilon_t, \quad \varepsilon_t \sim N(0, \Sigma_t) \quad (1)$$

let z_t , ε_t , and z_{t-i} (with $i = 1, \dots, p$) be $N \times 1$ dimensional vectors, where the time-varying VAR coefficient Π_{it} (with $i = 1, \dots, p$) and time-varying variance-covariance matrix Σ_t are $N \times N$ dimensional matrices. Using the lag operator to write Eq. (1), we have: $\Pi(L)z_t = \varepsilon_t$ where $\Pi(L)$ denotes the $(N \times N)$ matrix lag-polynomial: $\Pi(L) = [I_N - \Pi_{1t}L - \Pi_{2t}L^2 - \dots - \Pi_{pt}L^p]$ with I_N identity matrix. Following the Wold representation theorem, a TVP-VAR stationary process can be rewritten as a TVP – VMA(∞): $z_t = \Lambda(L)\varepsilon_t$, where $\Pi(L) = [\Lambda(L)]^{-1}$. Since the lag number of $\Lambda(L)$ is infinite, we computed Λ_h at $h=1, \dots, H$ horizons to approximately represent it (Chatziantoniou et al., 2023).

Next, we calculated generalized forecast error variance decomposition (GFEVD), which is interpreted as the impact of shocks in variable j on the variance of forecast errors in variable i through Λ_h . GFEVD can be expressed as:

$$C_{ijt}(H) = \frac{(\Sigma_t)_{jj}^{-1} \sum_{h=0}^H ((\Lambda_h \Sigma_t)_{ijt})^2}{\sum_{h=0}^H (\Lambda_h \Sigma_t \Lambda_h^T)_{ii}} \quad (2)$$

$$\tilde{C}_{ijt}(H) = \frac{C_{ijt}(H)}{\sum_{i=1}^N C_{ijt}(H)} \quad (3)$$

where $\tilde{C}_{ijt}(H)$ represents the contribution of the j th variable to the variance of the forecast error of the i th variable at horizon H . We normalized $\tilde{C}_{ijt}(H)$ and obtain: $\sum_{i=1}^N \tilde{C}_{ijt}(H) = 1$, $\sum_{j=1}^N \sum_{i=1}^N \tilde{C}_{ijt}(H) = N$.

Furthermore, based on Eqs. (2) and (3), we calculated all connectedness measures.

$$NPDC_{ijt}(H) = \tilde{C}_{ijt}(H) - \tilde{C}_{ji}(H) \quad (4)$$

$NPDC_{ijt}(H) > 0$ ($NPDC_{ijt}(H) < 0$) implies that the impact of variable j on variable i is stronger (weaker) than the impact of variable i on variable j . Here, $NPDC_{ijt}(H)$ is the key indicator for constructing the return connectedness network in this paper. Other connectedness measures are as follows:

The total directional connectedness of variable i transmits to other variables:

$$TO_{it}(H) = \sum_{j=1, j \neq i}^N \tilde{C}_{jit}(H) \quad (5)$$

The total directional connectedness of variable i receives from other variables:

$$FROM_{it}(H) = \sum_{j=1, j \neq i}^N \tilde{C}_{ijt}(H) \quad (6)$$

The net total directional connectedness of variable i :

$$NET_{it}(H) = TO_{it}(H) - FROM_{it}(H) \quad (7)$$

where $NET_{it}(H) > 0$ ($NET_{it}(H) < 0$) denotes that variable i acts as the net transmitter (net receiver) in the network of connectedness.

The total connectedness index (TACI) can be calculated by:

$$TACI_t(H) = \frac{1}{N} \sum_{i=1}^N TO_{it}(H) = \frac{1}{N} \sum_{i=1}^N FROM_{it}(H) \quad (8)$$

where $TACI_t(H)$ measures the average level of the network of connectedness, that is, the average impact of a given variable to other variables, or it received the average shock from other variables.

2.1.2. Frequency domain connectedness

Referencing the study of Baruník and Křehlík (2018), the frequency response function is written as $\Lambda(e^{-i\omega}) = \sum_{h=0}^{\infty} e^{-i\omega h} \Lambda_h$, where imaginary number $i = \sqrt{-1}$ and ω represents the frequency to continue with the spectral density of z_t at frequency ω . We defined the spectral density of z_t at frequency ω as a Fourier transformation of the TVP – VMA(∞):

$$S_z(\omega) = \sum_{h=-\infty}^{\infty} E(z_t z_{t-h}^T) e^{-i\omega h} = \Lambda(e^{-i\omega}) \Sigma_t \Lambda^T(e^{+i\omega}) \quad (9)$$

The frequency GFEVD, combining the spectral density and the GFEVD, can be denoted as follows:

$$C_{ijt}(\omega) = \frac{(\Sigma_t)_{jj}^{-1} \left[\left(\sum_{h=-\infty}^{\infty} e^{-i\omega h} \Lambda_h \Sigma_t \right)_{ijt} \right]^2}{\left(\Lambda(e^{-i\omega}) \Sigma_t \Lambda^T(e^{+i\omega}) \right)_{ii}} \quad (10)$$

$$\tilde{C}_{ijt}(\omega) = \frac{C_{ijt}(\omega)}{\sum_{i=1}^N C_{ijt}(\omega)} \quad (11)$$

where $C_{ijt}(\omega)$ represents the contribution of the j th variable to the variance of the forecast error of the i th variable at a given frequency ω . Then, we aggregated all frequencies for a selected bandwidth, $d = (a, b)$ satisfied $a, b \in (-\pi, \pi)$ and $a < b$. We have:

$$\tilde{C}_{ijt}(d) = \int_a^b \tilde{C}_{ijt}(\omega) d\omega \quad (12)$$

Next, the connectedness measure for a given frequency bandwidth d can be written as:

$$NPDC_{ijt}(d) = \Omega(d) [\tilde{C}_{ijt}(d) - \tilde{C}_{ji}(d)] \quad (13)$$

$$TO_{it}(d) = \Omega(d) \sum_{j=1, j \neq i}^N \tilde{C}_{jit}(d) \quad (14)$$

$$FROM_{it}(d) = \Omega(d) \sum_{j=1, j \neq i}^N \tilde{C}_{ijt}(d) \quad (15)$$

$$NET_{it}(d) = TO_{it}(d) - FROM_{it}(d) \quad (16)$$

$$TACI_t(d) = \frac{1}{N} \sum_{i=1}^N TO_{it}(d) = \frac{1}{N} \sum_{i=1}^N FROM_{it}(d) \quad (17)$$

where $\Omega(d) = \sum_{i,j=1}^N \tilde{C}_{ijt}(d) / N$. There is a conversion relationship between frequency-domain connectedness and time-domain connectedness:

$$Y(H) = \sum_d \left(\frac{1}{\Omega(d)} Y(d) \right), \quad \text{where } Y(\bullet) = \{ NPDC_{ijt}(\bullet), TO_{it}(\bullet), FROM_{it}(\bullet), NET_{it}(\bullet), TACI_t(\bullet) \}.$$

2.2. Multilayer dynamic connectedness network graph

We defined dynamic network G as a series of instantaneous snapshots

of the network, which is ordered by discrete timestamps on the sample time interval $[1, T]$ (Fig. 1) (Pedreschi et al., 2022). The dynamic network G be expressed as $G = \{G_0, G_1, G_2, \dots, G_T\}$. Each snapshot G_t is a static network at time t .

In order to identify the role played by crude oil, coal, natural gas, and power futures in the EFRCN, we considered the snapshot of the network as a directed multilayer EFRCN in this paper. According to Kivela et al. (2014), the directed multilayer EFRCN can be expressed as $G_t = (E_t, V_t, W_t, L)$ where E_t represents the edge set, V_t indicates the vertex set, W_t stands for the set of edge's weight, and L denotes the layer set (with $L = \{oil, coal, gas, power\}$). We defined the vertex set $V_t = \{V_t^L\}$ satisfied $V_t^g \cap V_t^h = \emptyset$ where $g, h \in L$ and $g \neq h$. Further, we defined the weight set $W_t = \{w_{ijt}\}$ where $i, j \in V_t^L$. The value of weight is expressed as $w_{ijt} = NPDC_{jit}$. E_t is a set of directed linkages between pairs of vertex-layer tuples, that is $E_t \subseteq V_t^p \times V_t^q$ (with $p, q \in L$). The element of the adjacency matrix e_{ijt} is defined as:

$$e_{ijt} = \begin{cases} 1, w_{ijt} > 0 \\ 0, w_{ijt} \leq 0 \end{cases} \quad (18)$$

$e_{ijt} = 1$ denotes the presence of a directed edge with a weight of w_{ijt} from vertex i points to vertex j in the network, and $e_{ijt} = 0$ implies the absence of the edge. Since $NPDC_{jit}$ and $NPDC_{itj}$ are a pair of opposite numbers, there is only a unidirectional edge between vertex i and j . Then, following the procedures employed by Restrepo et al. (2018) and Akyildirim et al. (2022), we removed the edges corresponding to their weight values that are less than the threshold of the bottom 10 percent quantiles of the set $\{w_{ijt} | w_{ijt} > 0\}$ from the graph. Heretofore, we have established a complete dynamic multilayer unidirectional network graph.

2.3. Detect changepoints of COVID-19 lockdown policies

We employed the Pruned Exact Linear Time (PELT) method proposed by Killick et al. (2012) to identify changepoints in the population and GDP under the COVID-19 lockdown. Formally, we considered a given sequence s_t representing the scale of population or GDP under lockdown, which is partitioned into $\lambda+1$ segments corresponding to λ changepoints, whose positions are denoted as $(\tau_1, \dots, \tau_\lambda)$. We specified the start position of the sequence as $\tau_0 = 0$ and the end position as $\tau_{\lambda+1} = n$, where n is the length of the series. In order to detect the number and positions of changepoints, we formulated the following optimization problem.

$$\min_{\lambda, \tau_{1:\lambda}} \sum_{i=1}^{\lambda+1} [C(s_{(\tau_{i-1}+1):\tau_i}) + \beta] \quad (19)$$

Here, $C(\bullet)$ is a cost function for a segment, and β is a penalty parameter to guard against overfitting.

In the Pelt algorithm, we applied the radial basis function (RBF) as the cost function (Truong et al., 2020). For each time point in the time series data, the Pelt algorithm calculates the cost value of the corresponding segmentation (i.e., the segmented subsequence) up to that time point. This cost value is computed using the RBF function, whose formula is given as follows:

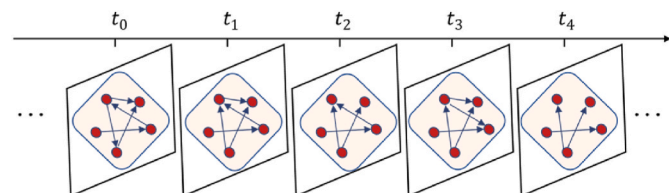


Fig. 1. The dynamic network concept.

$$C_t(j) = (j - t) \bullet \log(n - t) + \log \left[\sum_{i=t}^j \exp \left(- \frac{(s_i - s_t)^2}{2\sigma^2} \right) \right] \quad (20)$$

Here, t represents the current time point, j denotes the index of the last point from t , s_i represents the value of the i th data point, and σ is a parameter in RBF that controls the shape of the function. In this formula, the first term $(j - t) \bullet \log(n - t)$ is a penalty, which makes the model more inclined to choose segment schemes with fewer segments. The second term $\log \left[\sum_{i=t}^j \exp \left(- \frac{(s_i - s_t)^2}{2\sigma^2} \right) \right]$ measures the quality of the current segmentation, and the smaller it is, the better the current segmentation.

The PELT method uses a recursive approach to solve the above minimization problem (Killick et al., 2012). Let $\Xi(\xi)$ represent the minimized value for the data $y_{1:\xi}$ with the specified set of segmentation points $\Gamma_\xi = \{\tau : 0 = \tau_0 < \tau_1 < \dots < \tau_\lambda < \tau_{\lambda+1} = \xi\}$. Set $\Xi(0) = -\beta$. Then, we have:

$$\begin{aligned} \Xi(\xi) &= \min_{\tau \in \Gamma_\xi} \left\{ \sum_{i=1}^{\lambda+1} [C(s_{(\tau_{i-1}+1):\tau_i}) + \beta] \right\} \\ &= \min_t \left\{ \min_{\tau \in \Gamma_\xi} \sum_{i=1}^{\lambda} [C(s_{(\tau_{i-1}+1):\tau_i}) + \beta] + C(s_{(t+1):n}) + \beta \right\} \\ &= \min_t \{ \Xi(t) + C(s_{(t+1):n}) + \beta \} \end{aligned} \quad (21)$$

Here, $\xi = 1, 2, \dots, n$, subject to $t < \xi$ and $t \in \Gamma_\xi$.

3. Data source and variables definition

3.1. Data source

We collected data from the CoronaNet Research Project (Cheng et al., 2020)¹ and OxCGRT (Hale et al., 2021)² regarding COVID-19 lockdown policies implemented globally, as well as daily futures contract closing price data for four energy futures (crude oil, coal, natural gas, and electricity) with expiration dates in the latest month from the Bloomberg database. Details about the picked energy futures contracts are provided in Supplementary Table S1. The data spans the period from January 22, 2020, to December 24, 2021. To measure the impact of global COVID-19 lockdown interventions, we aggregated daily data on the population and GDP affected by the policies. For population aggregating, we utilized global administrative boundaries data from the GADM database (version 4.10) and population distribution data for various administrative levels from the LandScan database. The total daily GDP affected by the lockdown policy is calculated by multiplying the population of the lockdown area with the per capita GDP of that area. This provides an estimate of the economic impact of the lockdown policy on the lockdown area. The per capita GDP data has been sourced from the World Economic Outlook published by the IMF in October 2022.

3.2. Defining variables

3.2.1. Populations and GDP under COVID-19 lockdown

In this paper, we aggregated the population and GDP impacts of COVID-19 lockdown policies, which can serve as proxy indicators for measuring the intensity of COVID-19 lockdowns globally (Fig. 2). Firstly, we collected information sets for each lockdown policy, including the start and end dates of the policy, the administrative region level affected by the policy, the population categories targeted by the

¹ <https://www.coronanet-project.org>.

² <https://www.bsg.ox.ac.uk/covidtracker>.

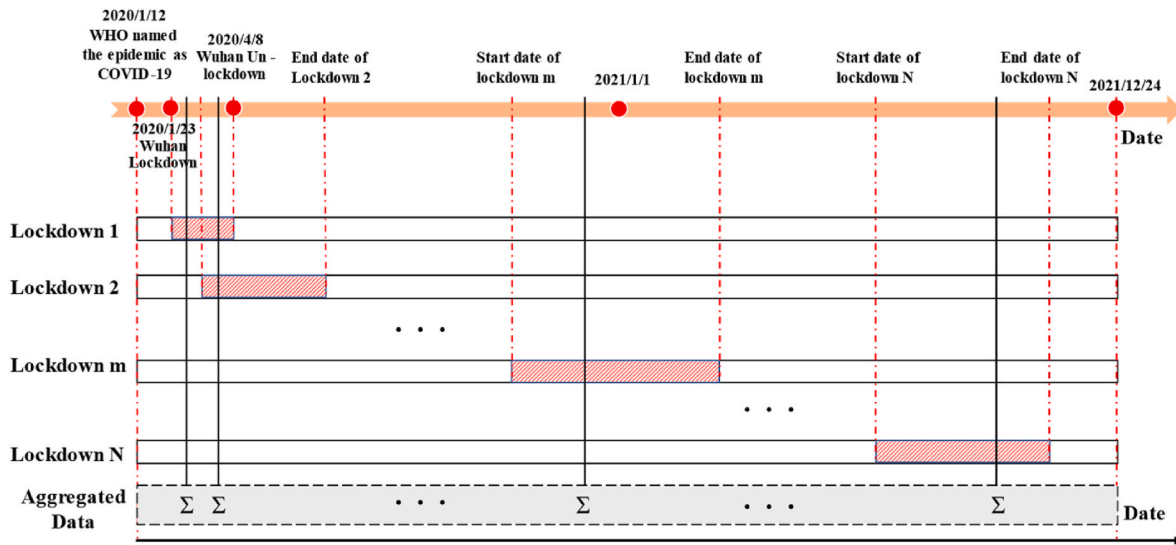


Fig. 2. The process of aggregating population and economic scales impacted by COVID-19 lockdown policies.

policy, and so on. We excluded lockdown policies targeting specific groups, such as healthcare workers and students, as we focused on policies targeting the general public. After applying the filters mentioned above, we obtained a total of 2972 COVID-19 lockdown policies worldwide.

Secondly, government entities with administrative subordination often implement COVID-19 lockdown policies simultaneously for a certain period. In such cases, we refer to the lockdown policy implemented by the higher-level government entity as the “parent lockdown” and the one implemented by the lower-level government entity as the “child lockdown”. To avoid duplicate calculations caused by administrative subordination in the subsequent aggregating process, we removed the periods where the child lockdown overlapped with the parent lockdown. For example, Wuhan City implemented the COVID-19 lockdown policy throughout the city from January 23, 2020 to April 8, 2020, while the Jiangnan District under Wuhan City also implemented a lockdown policy during this period. Therefore, the parent lockdown policy implemented by Wuhan City and the child lockdown policy implemented by Jiangnan District overlap in terms of dates. We removed the overlapping dates by adjusting the start time of the child lockdown policy.

Next, we obtained population data corresponding to the administrative region scope of each lockdown policy implemented from the GADM and LandScan databases. At the same time, we calculated the GDP scale corresponding to each lockdown policy’s administrative region by using the region’s per capita GDP multiplied by the number of people affected by the lockdown.

Finally, we mapped the date range of each lockdown policy onto the date axis and aggregated the daily population and GDP impacts of the COVID-19 lockdowns. Fig. 2 shows two date axes and several vertically arranged bands, each corresponding to a lockdown policy. The red-shaded part of the policy band represents the time interval during which the lockdown policy was in effect on the time axis. The symbol “Σ” in the gray area at the bottom represents the daily summation of the results.

Fig. 3 depicts a remarkable similarity in the temporal evolution of population and GDP impacted by COVID-19 lockdown policies. The figure also showcases a pronounced peak during March–June 2020 and additional small peaks, such as during August–September 2020 and November 2020–January 2021, among others.

3.2.2. Statistical characteristics of EFRCN

A 4-layer temporal network graph of energy futures return

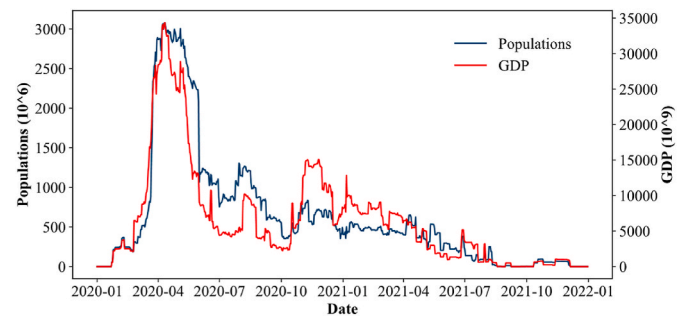


Fig. 3. Aggregated Population and GDP Scale impact of COVID-19 Lockdown policies.

connectedness was constructed in our work. The indicators of the network graph contain two main categories: global network indicators and local network indicators. The global network indicators include average strength, graph density, and average weighted clustering coefficient, while the local network indicators mainly consist of a hierarchical ratio of out-strength and in-strength, including crude oil futures, coal futures, natural gas futures, and power futures. The network is divided into short-term, long-term, and non-periodic temporal network graphs according to the time scale. The calculation processes of network structural indicators are described in the following.

3.2.2.1. Average strength. Next, we introduced some statistical characteristics of established complex networks. Drawing on the concepts of in-strength and out-strength, as outlined by Chen et al. (2018), as well as the notion of node average strength, as employed by Wang et al. (2019), we defined statistical indicators for the average out-strength and average in-strength of the EFRCN to reflect the level of information flow in the network at time t .

$$\text{Average out-strength}_i = \frac{1}{n} \sum_{i=1}^n \sum_j^{t_i} w_{ij} * e_{ij} \quad (22)$$

$$\text{Average in-strength}_i = \frac{1}{n} \sum_{i=1}^n \sum_j^{r_i} w_{ji} * e_{ji} \quad (23)$$

where n represents the number of vertices in the network, t_i represents the number of directed edges emanating from vertex i , and r_i indicates

the number of directed edges through which vertex i receives information.

For a unidirectional weighted network graph, there is at most one directed weighted edge between any two selected vertices i and j . Thus, the average out-strength of the network is equivalent to the average in-strength. Considering this, we introduced the statistical indicator for the average strength of the network.

$$Averagestrength_t = \frac{1}{n} \sum_{i=1}^n \sum_j^{i_i} w_{ijt} * e_{ijt} \quad (24)$$

3.2.2.2. Intra-layer ratio of average out-strength and average in-strength.

In this study, we constructed a unidirectional weighted connectedness network for energy futures market return that consists of four layers, denoted as $L = (oil, coal, gas, power)$. Each layer represents a specific energy futures market, and its vertices are selected energy futures series. To measure the relative strength of return spillovers in each layer, we introduced a new statistical indicator: the ratio of a network layer's out-strength to its in-strength at time t .

$$Out - in - ratio_{l,t} = \frac{Out - strength_{l,t}}{In - strength_{l,t}} = \frac{\sum_{i=1}^{n_l} \sum_j^{i_l} w_{ijt} * e_{ijt}}{\sum_{y=1}^{r_l} \sum_x^{r_l} w_{xyt} * e_{xyt}}, (i, y \in V^l) \quad (25)$$

Here, l represents a specific network layer, and n_l denotes the number of vertices within that layer l , r_y is the number of directed edges point to vertex y . $Out - in - ratio_{l,t} > 1$ indicates that, on average, network layer l acts as a net spillover of return information in the network graph at time t . Conversely, $Out - in - ratio_{l,t} < 1$ indicates that network layer l acts as a net receiver of return information in the network graph at time t . $Out - in - ratio_{l,t} = 1$ implies a net spillover effect of zero within the network layer l at time t . Evidently, a prerequisite for the applicability of this novel statistical indicator relies on the non-zero nature of the denominator in Eq. (25), implying that within a specified network layer denoted as l , there must exist at least one vertex receiving spillover information originating from other vertices.

3.2.2.3. Network sparsity. The network density is a measure of the sparsity of a network graph, defined as the ratio of the number of edges in the graph to the maximum number of possible edges that could exist between the vertices (Boccaletti et al., 2014).

$$density_t = \frac{Edge\ Number_t}{n(n-1)/2} \quad (26)$$

where n and $Edge\ Number_t$ are the number of vertices and edges at time t , respectively.

3.2.2.4. Average weighted clustering coefficient. To measure the cluster structure characteristics of the network graph, we calculated the average weighted clustering coefficient, $Clustering$, which is defined as the mean of the weighted clustering coefficients of all network vertices (Wang et al., 2019). The vertex's weighted clustering coefficient C_{it}^w measures the local cohesiveness in the vertex i 's neighborhood, and its measure is based on Barrat et al. (2004).

$$Clustering_t = \frac{\sum_{i=1}^n C_{it}^w}{n} = \frac{1}{n} \sum_{i=1}^n \left[\frac{1}{s_{it}(k_{it}-1)} \sum_{j,h} \frac{(w_{ijt}^* + w_{iht}^*)}{2} e_{ijt}^* e_{iht}^* \right] \quad (27)$$

Here, s_{it} represents the sum of the out-strength and in-strength of vertex i at time t , which indicates the strength of the vertex. k_{it} is the number of vertices that vertex i connects to. Additionally, we defined $w_{ijt}^* = |w_{ijt}|$, and $e_{ijt}^* = 1$ when $e_{ijt} = 1$ or $e_{jit} = 1$. The names of all variables and their corresponding labels are presented in Table 1.

Table 1

List of variables.

Variable name	Label	Variable name	Label
Populations under COVID-19 lockdown	Popc	Out-in-ratio of crude oil markets	Oiro
GDP under COVID-19 lockdown	Gdpc	Out-in-ratio of crude oil markets in short-term	Oiro_s
Average strength	Avsn	Out-in-ratio of crude oil markets in long-term	Oiro_l
Average strength in short-term	Avsn_s	Out-in-ratio of coal markets	Oirc
Average strength in long-term	Avsn_l	Out-in-ratio of coal markets in short-term	Oirc_s
Graph density	Gden	Out-in-ratio of coal markets in long-term	Oirc_l
Graph density in short-term	Gden_s	Out-in-ratio of natural gas markets	Oirn
Graph density in long-term	Gden_l	Out-in-ratio of natural gas markets in short-term	Oirn_s
Average weighted clustering coefficient	Awcc	Out-in-ratio of natural gas markets in long-term	Oirn_l
Average weighted clustering coefficient in short-term	Awcc_s	Out-in-ratio of power markets	Oirp
Average weighted clustering coefficient in long-term	Awcc_l	Out-in-ratio of power markets in short-term	Oirp_s
		Out-in-ratio of power markets in long-term	Oirp_l

4. Results and discussion

4.1. Preliminary analysis

4.1.1. Descriptive statistics of variables

The descriptive statistics of all variables are presented in Table 2. We observed that the coefficient of variation of $Popc_t$ and $Gdpc_t$ is greater than 1, while all the network structural indicators are less than 1. This indicates that the distribution of data points for $Popc_t$ and $Gdpc_t$ are more dispersed compared to the data for network structural indicators. Skewness values of $Gden_t$, $Gden_s_t$, $Awcc_s_t$, $Gden_l_t$, and $Awcc_l_t$ are less than 0, indicating that their distributions of sample points exhibit left-skewed characteristics. However, the distributions of the remaining variables exhibit right-skewed tendencies. The Jarque-Bera tests show that, except for the variables $Awcc_t$ and $Awcc_s_t$, all other variables reject the assumption of normality at the 1% significance level. The ADF test indicates that $Popc_t$, $Gdpc_t$, $Oirn_t$, $Oirn_s_t$, $Oirp_s_t$, $Oirn_l_t$, and $Oirp_l_t$ are non-stationary, while the remaining variables reject the null hypothesis of the existence of unit roots at least at the 10% significance level. Therefore, we considered these variables to be stationary. The Ljung-Box test results indicate that all variables reject the null hypothesis at the 1% level, representing that all variables are non-random variables, i.e., all variables are non-white noise series.

For the non-stationary variables, the test results show that the first-order difference of all non-stationary time series is stationary and non-white noise (refer to Supplementary Table S2). Meanwhile, the E-G two-step tests illustrate that there is no cointegration relationship between $Popc_t$ and $Gdpc_t$ and other non-stationary series (refer to Supplementary Table S3). Therefore, in subsequent empirical analysis, we used the first-order difference sequence of the non-stationary series instead of the original series.

4.1.2. Correlation analysis

Fig. 4 presents the results of the variable correlations. The lower triangular area of the figure shows the numerical results of the correlation matrix, while the upper triangular area shows the visual results of variable correlation coefficients and corresponding significance. Observing the visual results in the first row, we found that variable $D.Popc_t$ has a significant positive correlation at the 1% level with variables $Gden_t$, $Awcc_t$, $Oiro_t$, $Oirc_t$, $Oirp_t$, $Gden_s_t$, $Awcc_s_t$, $Avsn_s_t$, $Oiro_s_t$, $Oirc_s_t$, $D.Oirp_s_t$, $Avsn_l_t$, and $Oiro_l_t$, while having a significantly

Table 2

Descriptive statistics of network indicators and the scale of GDP and populations impacted by the COVID-19 lockdown.

Variable	Mean	Std. D.	Co. var.	Skew.	Kurt.	JB	ADF	L-B
$Popc_t$	654.051	754.621	1.154	1.953	3.113	516.360***	-1.487	5238.567***
Gdp_c_t	6718.790	7363.424	1.096	1.865	3.328	516.711***	-2.200	5080.839***
$Gden_t$	0.439	0.020	0.046	-0.801	2.957	232.104***	-3.626***	3055.124***
$Awcc_t$	0.895	0.030	0.033	0.033	0.536	5.739	-3.728***	2864.306***
$Avsn_t$	9.999	0.854	0.085	0.814	0.145	55.668***	-3.009**	4144.584***
$Oiro_t$	0.806	0.130	0.161	0.386	1.779	76.753***	-3.169**	3490.801***
$Oirc_t$	0.462	0.179	0.387	2.352	20.504	9106.683***	-2.789*	2936.598***
$Oirn_t$	2.550	1.088	0.427	0.721	-0.284	45.205***	-2.168	4794.080***
$Oirp_t$	1.534	0.366	0.239	0.564	-0.428	30.545***	-2.635*	4372.353***
$Gden_{-s_t}$	0.442	0.019	0.044	-0.614	1.202	60.616***	-3.714***	3114.497***
$Awcc_{-s_t}$	0.898	0.028	0.031	-0.144	0.343	3.984	-3.864***	2726.001**
$Avsn_{-s_t}$	8.648	0.790	0.091	0.625	-0.371	35.648***	-2.992**	4168.956***
$Oiro_{-s_t}$	0.782	0.123	0.158	0.364	1.229	41.598***	-4.317***	3291.511***
$Oirc_{-s_t}$	0.466	0.169	0.362	2.315	22.340	10710.963***	-2.824*	2814.926***
$Oirn_{-s_t}$	2.052	0.899	0.438	0.999	0.700	93.054***	-2.202	4669.425***
$Oirp_{-s_t}$	1.779	0.444	0.250	0.718	-0.620	51.292***	-2.426	4617.153***
$Gden_{-l_t}$	0.443	0.017	0.038	-0.957	1.399	116.134***	-2.923**	2297.030***
$Awcc_{-l_t}$	0.905	0.028	0.031	-0.614	0.316	33.429***	-3.479***	2124.314***
$Avsn_{-l_t}$	1.837	0.212	0.115	1.610	4.065	554.605***	-2.908**	3440.234***
$Oiro_{-l_t}$	0.972	0.208	0.214	0.148	0.890	17.689***	-3.37**	3871.558***
$Oirc_{-l_t}$	0.582	0.363	0.623	2.187	5.134	939.487***	-2.795*	3881.833***
$Oirn_{-l_t}$	7.252	3.701	0.510	0.765	-0.311	51.038***	-2.286	4517.419***
$Oirp_{-l_t}$	0.715	0.217	0.303	0.295	-0.712	18.038***	-2.039	4475.661***

Note: Std. D., Co. var., Skew., and Kurt. are the abbreviations for standard deviation, coefficient of variation, skewness, and kurtosis, respectively. JB, ADF, and L-B represent Jarque-Bera test of normality, Augmented Dickey-Fuller test of stationarity, and Ljung-Box test of randomness, respectively. *, **, and *** denote statistical significance at the 10%, 5%, and 1% levels, respectively.

negative correlation with variables $D.Oirn_t$, $D.Oirn_{-s_t}$ and $D.Oirp_{-l_t}$, and no significant correlation with other variables. The second row of visual results for variable $D.Gdpc_t$ shows similar correlations with all variables in the first row. Therefore, summarizing these correlation results, three principal findings aligned with the objectives of the work are tentatively formulated. Firstly, a significant statistical correlation emerges between the change in COVID-19 lockdown intensity and the evolutionary trajectory of EFRCN’s topological structure. Secondly, in comparison to the long-term EFRCN, the associations between COVID-19 lockdown intensity and network indicators within the non-periodic EFRCN and short-term EFRCN exhibit heightened prominence. Thirdly, correlation results reveal differences in the linkages between COVID-19 lockdown intensity and the ratio of average out-strength to average in-strength across diverse energy futures markets.

4.2. COVID-19 lockdown policies and dynamic network

4.2.1. Estimating model

In this section, we examined the relationship between $Gdpc_t$, $Popc_t$, and the network structure indicators of the EFRCN. First, we established a benchmark model with the following form:

$$y_t = \beta_0 + \beta_1 x_t + u_t, t = 1, 2, \dots, T \tag{28}$$

Here, y_t represents the structure indicators of the EFRCN, x_t represents either $D.Gdpc_t$ or $D.Popc_t$, u_t is the residual, T is the length of the sample sequence, and β_0 and β_1 are parameters.

However, the regression results of the benchmark model are not robust because the residuals u_t have severe serial correlation due to the omission of many factors that affect the dependent variable. Therefore, we built a modified model as follows:

$$y_t = \beta_0 + \beta_1 x_t + u_t, t = 1, 2, \dots, T \tag{29}$$

$$u_t = \sum_{i=1}^p \alpha_i u_{t-i} + \varepsilon_t \tag{30}$$

Substituting Eq. (30) into Eq. (29), we obtained:

$$y_t = \beta_0 + \beta_1 x_t + \sum_{i=1}^p \alpha_i (y_{t-i} - \beta_0 - \beta_1 x_{t-i}) + \varepsilon_t \tag{31}$$

Here, ε_t is the residual term of the modified model, $\alpha_i (i = 1, \dots, p)$ are the parameters of the AR(p) model, and p is the minimum lag order that ensures the absence of serial correlation in ε_t . We employed the Gauss-Newton algorithm to iteratively estimate the parameters in Eq. (31) (Durbin, 1960).

4.2.2. Regression results and discussion

Tables 3–5 display the results of regression for network structural variables corresponding to non-periodic, short-term, and long-term scenarios, respectively. In Panel A of Table 3, we observed that the coefficients of $D.Gdpc_t$ in columns (I), (II), and (III) are statistically significant at a minimum of 5% level, which suggests that the average density, average weighted clustering coefficient, and average strength of the connectedness network of energy futures return are positively related to the GDP scale impacted by the global COVID-19 lockdown. These findings indicate that the lockdown policies implemented globally to contain COVID-19 have reinforced the connectedness of energy futures markets. The potential reasons behind this outcome can be attributed to at least three main factors. Firstly, the imposition of lockdown measures could exacerbate volatility in the energy futures markets. This phenomenon arises due to the reduced frequency of offline activities among investors during lockdowns, leading them to allocate more time and attention to engage in online trading activities (Guzmán et al., 2021). Consequently, there is an increased frequency of online trading, characterized by heightened buying and selling, which undoubtedly contributes to heightened market volatility. Secondly, lockdowns could trigger elevated panic sentiments among residents, and investors are no exception. Such panic-driven emotions might cause deviations from rational investor behavior (Chen et al., 2022b). Thirdly, lockdowns might result in a convergence of pessimistic expectations among investors, leading to spontaneously similar investment decisions. This alignment of decisions could subsequently enhance co-movement within the energy futures markets.

Moreover, the remaining columns in Panel A of Table 3 show that the coefficient of $D.Gdpc_t$ in column (IV) is significantly positive at the 1% level, while the coefficient in column (VII) is significant at the 10% level. These results imply that the net spillover effects of oil and electricity futures in the energy futures return connectedness network have

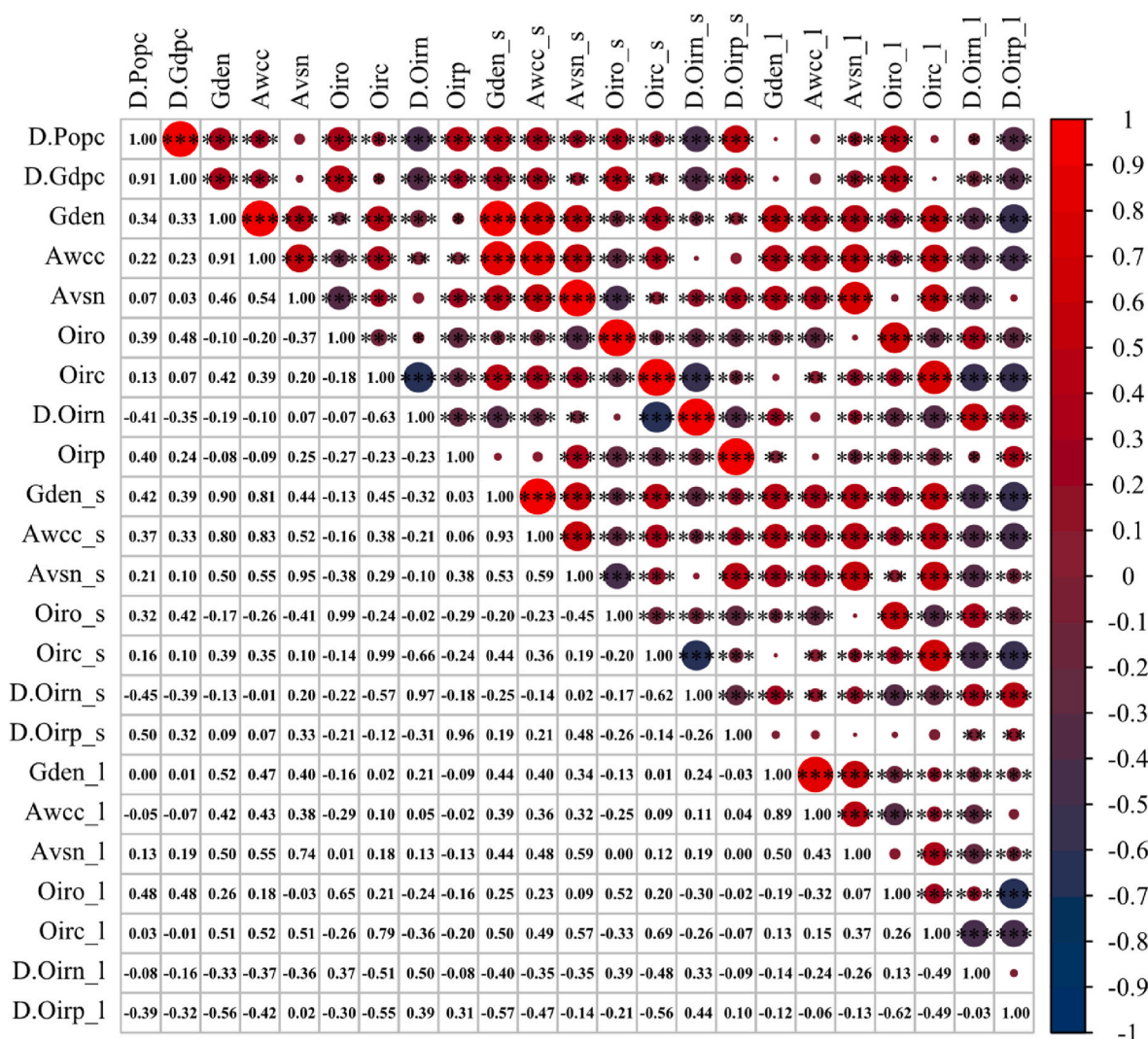


Fig. 4. Heatmap of correlation coefficients. Note: *, **, and *** denote statistical significance at the 10%, 5%, and 1% levels, respectively. The prefix “D.” in a variable name represents the first-order difference of this variable.

Table 3
Impact of the scale of populations and GDP under COVID-19 lockdown on structure of non-periodic EFRCN.

Panel A:	Dependent variables:						
	<i>Gden_t</i> (I)	<i>Awcc_t</i> (II)	<i>Avsn_t</i> (III)	<i>Oiro_t</i> (IV)	<i>Oirc_t</i> (V)	<i>D.Oirn_t</i> (VI)	<i>Oirp_t</i> (VII)
<i>D.Gdpc_t</i>	0.016 *** (3.430)	0.031 ** (2.093)	0.457 *** (4.119)	0.156 *** (5.869)	-0.061 * (-1.689)	-0.003 ** (-1.978)	0.059 * (1.851)
constant	0.439 *** (79.226)	0.895 *** (133.057)	10.045 *** (28.176)	0.801 *** (17.515)	0.475 *** (4.684)	-0.004 (-0.389)	1.474 *** (9.719)
p	2	2	2	1	4	1	2
D.W.	2.020	2.083	2.012	2.028	2.008	2.017	1.991
F-statistic	689.684 ***	410.377 ***	1246.808 ***	1552.907 ***	199.241 ***	65.365 ***	1801.118 ***
A. R ²	0.846	0.766	0.909	0.903	0.704	0.205	0.935
Panel B:							
<i>D.Pop_t</i>	0.105 *** (2.916)	0.225 * (1.884)	2.832 *** (6.433)	0.887 *** (3.118)	-0.423 (-1.564)	-0.021 * (-1.792)	0.391 * (1.691)
constant	0.439 *** (78.984)	0.895 *** (115.106)	10.046 *** (28.072)	0.8 *** (13.814)	0.471 *** (4.993)	-0.004 (-0.421)	1.474 *** (9.719)
p	2	3	2	3	3	2	2
D.W.	2.021	2.008	2.011	1.998	2.076	1.994	1.991
F-statistic	689.538 ***	337.52 ***	1252.45 ***	1182.08 ***	232.254 ***	47.314 ***	1801.407 ***
A. R ²	0.846	0.771	0.909	0.904	0.698	0.217	0.935

Table 4
Impact of the scale of populations and GDP under COVID-19 lockdown on structure of short-term EFRCN.

Panel A:	Dependent variables:						
	<i>Gden_{s,t}</i> (I)	<i>Awcc_{s,t}</i> (II)	<i>Avsn_{s,t}</i> (III)	<i>Oiro_{s,t}</i> (IV)	<i>Oirc_{s,t}</i> (V)	<i>D.Oirn_{s,t}</i> (VI)	<i>D.Oirp_{s,t}</i> (VII)
<i>D.Gdpc_t</i>	0.014 ** (2.396)	0.024 ** (2.202)	0.146 *** (3.31)	0.137 ** (2.04)	-0.051 * (-1.711)	-0.003 * (-1.687)	0.017 *** (5.111)
constant	0.442 *** (87.238)	0.898 *** (187.016)	8.677 *** (28.42)	0.774 *** (14.689)	0.473 *** (5.226)	-0.004 (-0.468)	0.001 (0.214)
p	2	1	1	3	3	2	2
D.W.	2.013	2.086	2.039	1.993	2.071	1.998	1.986
F-statistic	622.534 ***	476.468 ***	2002.704 ***	884.055 ***	213.667 ***	40.42 ***	303.302 ***
A. R ²	0.833	0.74	0.923	0.898	0.68	0.191	0.645
Panel B:							
<i>D.Pop_t</i>	0.107 *** (4.932)	0.145 *** (2.688)	0.824 ** (2.463)	0.712 *** (2.965)	-0.333 (-1.454)	-0.019 * (-1.682)	0.13 *** (5.074)
constant	0.442 *** (87.621)	0.898 *** (141.253)	8.677 *** (29.117)	0.775 *** (17.032)	0.473 *** (5.211)	-0.004 (-0.504)	0.001 (0.222)
p	2	2	1	2	3	1	1
D.W.	2.011	2.028	2.042	2.001	2.071	1.999	1.994
F-statistic	630.259 ***	405.898 ***	2004.12 ***	1096.234 ***	213.703 ***	42.613 ***	298.19 ***
A. R ²	0.834	0.764	0.923	0.898	0.68	0.143	0.543

Table 5
Impact of the scale of populations and GDP under COVID-19 lockdown on structure of long-term EFRCN.

Panel A:	Dependent variables:						
	<i>Gden_{l,t}</i> (I)	<i>Awcc_{l,t}</i> (II)	<i>Avsn_{l,t}</i> (III)	<i>Oiro_{l,t}</i> (IV)	<i>Oirc_{l,t}</i> (V)	<i>D.Oirn_{l,t}</i> (VI)	<i>D.Oirp_{l,t}</i> (VII)
<i>D.Gdpc_t</i>	0.009 ** (1.961)	0.013 ** (2.42)	0.293 * (1.85)	0.191 *** (2.967)	-0.016 (-1.496)	-0.002 *** (-2.686)	0.009 * (1.649)
constant	0.441 *** (106.35)	0.902 *** (126.134)	1.834 *** (19.817)	0.993 *** (12.98)	0.648 *** (3.215)	0.005 (0.155)	0.001 (0.332)
p	2	3	3	2	3	1	1
D.W.	2.022	2.013	1.995	2.003	2.043	2.041	2.043
F-statistic	422.569 ***	266.428 ***	509.492 ***	1225.402 ***	699.399 ***	68.451 ***	235.131 ***
A. R ²	0.771	0.726	0.836	0.907	0.875	0.212	0.484
Panel B:							
<i>D.Pop_t</i>	0.062 ** (2.172)	0.074 ** (2.06)	1.983 *** (3.491)	1.268 ** (2.216)	-0.097 (-1.571)	-0.013 (-1.601)	0.064 *** (7.131)
constant	0.441 *** (106.252)	0.903 *** (144.234)	1.834 *** (19.784)	0.993 *** (13.008)	0.648 *** (3.209)	0.004 (0.133)	0.001 (0.322)
p	2	2	3	2	3	2	1
D.W.	2.022	2.052	1.995	2.004	2.042	1.996	2.042
F-statistic	422.587 ***	328.727 ***	509.828 ***	1219.013 ***	699.885 ***	56.246 ***	352.476 ***
A. R ²	0.771	0.724	0.836	0.907	0.875	0.249	0.584

increased as the GDP scale affected by the global COVID-19 lockdown increases. One possible reason for this change is that the global COVID-19 lockdown has caused a supply shock to oil, exacerbating the imbalance between oil supply and demand, driving up oil prices, and thus enhancing the net spillover effects of oil in the entire energy return network system. The strengthening of the net spillover effects of electricity futures may be due to the demand shock caused by the COVID-19 pandemic. Additionally, the coefficient of *D.Gdpc_t* in column (V) is significantly negative at the 10% level, while the coefficient in column (VI) is significant at the 5% level, indicating that the net spillover effects of coal and natural gas futures in the energy futures return connectedness network decrease as the GDP scale affected by the global COVID-19 lockdown increase. In summary, the results suggest that the increasing intensity of the global COVID-19 lockdown has strengthened the net spillover effects of oil and electricity futures in the EFRCN, while weakening the net spillover effects of coal and natural gas futures.

Comparing the coefficients of *D.Gdpc_t* in each column of Panel A in Table 3 with the corresponding columns in Panel B of Table 3, we found that most of the signs of the *D.Pop_t* coefficients remain unchanged. The only notable difference is that the coefficient of *D.Pop_t* in column (V) in Panel B of Table 3 is not statistically significant, while the coefficients in other columns are significant at a minimum of 10% level. The findings presented in Table 4 are similar to those in Table 3. In Table 5, the coefficients of *D.Gdpc_t* and *D.Pop_t* in column (V) are not statistically

significant, indicating that the increasing intensity of the lockdown does not significantly reduce the net spillover effect of coal futures in the long-term energy futures return connectedness network. Additionally, the coefficient of *D.Pop_t* in column (VI) is not significant, suggesting that the increasing population controlled due to the global COVID-19 lockdown does not significantly reduce the net spillover effects of natural gas futures in the long-term return connectedness network.

4.3. COVID-19 lockdown policy changepoints and network structure

4.3.1. Identifying changepoints of COVID-19 lockdown policies

As the COVID-19 pandemic continues to develop globally, intervention policies aimed at preventing its spread have been dynamically adjusted. In this study, we utilized the PELT algorithm to pinpoint the turning points of COVID-19 lockdown policies worldwide. Fig. 5 shows that the variables *Pop_t* and *Gdpc_t* are segmented into seven segments, with the start and end dates of each segment displayed in Table 6.

By analyzing the segmentation results, we observed that the lengths of the first four segments are relatively short, whereas the last three segments are markedly longer. This suggests that the transition of COVID-19 lockdown policies was more frequent in the early stages of the pandemic, whereas the global lockdown policies were more stable in the middle and later stages of the pandemic. This can be attributed to the fact that, during the early stage of the COVID-19 outbreak, countries had

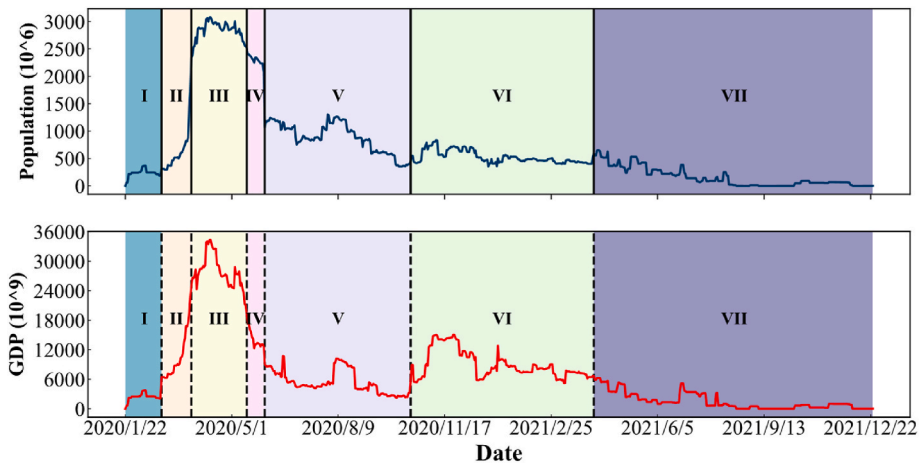


Fig. 5. Changepoints and segments of GDP and populations impacted by COVID-19 lockdown policies.

Table 6
Start and end date of the segments.

Segment	I	II	III	IV	V	VI	VII
Start date	2020/1/22	2020/2/24	2020/3/23	2020/5/14	2020/5/31	2020/10/15	2021/4/5
End date	2020/2/24	2020/3/23	2020/5/14	2020/5/31	2020/10/15	2021/4/5	2021/12/24

not yet established complete intervention strategies to prevent the rapid spread of the virus. As a result, lockdown policies were widely adopted by governments worldwide to curb the virus’s spread. However, in response to the disruptions caused by lockdowns to people’s work and daily lives, authorities in various countries rapidly adjusted their epidemic prevention and control strategies, gradually shifting towards other milder types of intervention policies. Therefore, after the fourth segment, both the population and GDP controlled by COVID-19 lockdown policies have significantly decreased, and the duration of each segment has become considerably longer.

4.3.2. Empirical strategy

During the sample period, we constructed a digital index for dates, with the start date assigned an index of 0 and the end date assigned an index of N . $Popc_t$ or $Gdpc_t$ is partitioned into $m+1$ segments by m changepoints $\tau_1, \tau_2, \dots, \tau_m$. The set of changepoints is represented as $\tau = \{0 = \tau_0 < \tau_1 < \dots < \tau_m < \tau_{m+1} = N\}$, where τ_0 represents the start date and τ_{m+1} denotes the end date.

Next, we investigated whether there are significant changes in the evolution process of network structural indicators at each changepoint. First, we divided the specific series of network structure indicator y_t into $m+1$ segments based on the m changepoints. We then concatenated the two adjacent segments to changepoint j to obtain a subsequence $y_{jt} =$

$y_{(\tau_{j-1}+1):(\tau_{j+1}-1)}$, where $j= 1, 2, \dots, m$ (see Fig. 6). Finally, we constructed a breakpoint autoregressive model AR(p) to identify the effects at the changepoints. The model is formulated as follows:

$$y_{jt} = \alpha_j + \beta_{0j} * D_{jt} + \sum_{i=1}^p \beta_{1ji} y_{j,t-i} + \sum_{i=1}^p (\beta_{2ji} * D_{jt}) y_{j,t-i} + \epsilon_{jt}$$

$$= (\alpha_j + \beta_{0j} * D_{jt}) + \sum_{i=1}^p (\beta_{1ji} + \beta_{2ji} * D_{jt}) y_{j,t-i} + \epsilon_{jt} \tag{32}$$

Here, $\alpha_j, \beta_{0j}, \beta_{1ji}$, and β_{2ji} are the parameters to be estimated. D_{jt} is a dummy variable that can be expressed as:

$$D_{jt} = \begin{cases} 0, & \tau_{j-1}+1 \leq t \leq \tau_j \\ 1, & \tau_j < t \leq \tau_{j+1}-1 \end{cases} \tag{33}$$

4.3.3. Regression results and discussion

Utilizing the empirical strategy mentioned above, we studied whether the evolution trends of global network structural indicators experience alterations at the changepoints. For this study, we chose a maximum lag order of 2 for the variable y_{jt} , which ensures that all residual series resulting from autoregressive modeling of selected variables exhibit white noise properties. In this empirical analysis, our primary focus is on examining the coefficient and corresponding significance level of the dummy variable D_t and the interaction between the dummy variable D_t and y_{jt-i} . The regression results of non-periodic, short-term, and long-term global network structural variables are presented in Tables 7–9, respectively.

In the first part of Table 7, we presented the regression results of subsequence y_{jt} , which are generated by concatenating the j th and $(j+1)$ th segments of variable $Gden_t$, in columns (j) for $j = 1, 2, \dots, 6$. The results in column (I) show that the coefficients of $D_t, D_t \times y_{jt-1}$, and $D_t \times$

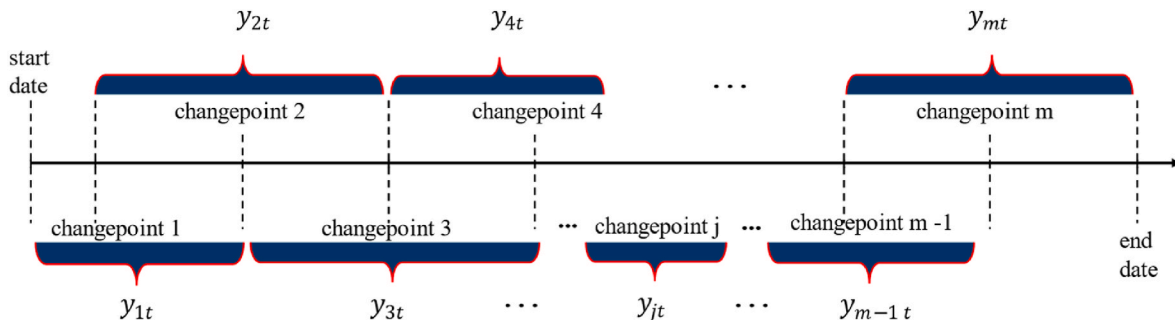


Fig. 6. The splicing process of adjacent segments.

Table 7
Evolution trend of non-periodic EFRCN's global structural indicators near policy changepoints.

$y_t : Gden_t$	y_{1t}	y_{2t}	y_{3t}	y_{4t}	y_{5t}	y_{6t}
	(I)	(II)	(III)	(IV)	(V)	(VI)
D_t	0.068*** (3.298)	0.003 (1.084)	0.126** (2.167)	-0.093 (-1.646)	0.007** (2.479)	-0.022** (-2.076)
$D_t \times y_{jt-1}$	0.399** (2.102)	0.270*** (3.886)	0.187*** (3.471)	-0.124*** (-3.584)	-0.064 (-1.617)	-0.100 (-1.492)
$D_t \times y_{jt-2}$	0.024* (1.747)	0.053* (1.906)	0.369 (1.083)	0.337 (1.457)	-0.085 (-1.544)	-0.050 (-1.359)
Others	Control	Control	Control	Control	Control	Control
F-statistic	7.676***	5.741***	6.876***	36.647***	96.561***	145.681***
$y_t : Awcc_t$						
D_t	0.016** (2.127)	0.069* (1.776)	-0.122 (-1.610)	-0.106 (-1.537)	-0.073 (-1.488)	0.052 (1.348)
$D_t \times y_{jt-1}$	0.139*** (2.862)	0.432* (1.707)	0.288*** (3.678)	-0.331 (-1.393)	0.128 (1.461)	0.231 (1.319)
$D_t \times y_{jt-2}$	0.164** (2.527)	0.251** (2.27)	0.381 (1.589)	0.453 (1.63)	-0.101 (-1.555)	-0.133 (-1.568)
Others	Control	Control	Control	Control	Control	Control
F-statistic	14.827***	16.292***	10.563***	27.890***	90.979***	118.903***
$y_t : Avsn_t$						
D_t	-0.086* (-1.958)	-0.040 (-1.555)	0.206** (2.204)	-0.169*** (-2.728)	0.028 (1.372)	0.036 (1.315)
$D_t \times y_{jt-1}$	0.398** (2.214)	-0.172* (-1.909)	0.356** (2.098)	-0.627*** (-3.051)	0.296 (1.338)	-0.156 (-1.220)
$D_t \times y_{jt-2}$	0.565* (1.714)	0.372** (2.325)	1.167** (2.353)	-1.208*** (-3.412)	0.163 (1.2)	-0.272 (-1.496)
Others	Control	Control	Control	Control	Control	Control
F-statistic	11.168***	13.073***	7.804***	40.324***	14.108***	23.467***

Table 8
Evolution trend of short-term EFRCN's global structural indicators near policy changepoints.

$y_t : Gden_{-s_t}$	y_{1t}	y_{2t}	y_{3t}	y_{4t}	y_{5t}	y_{6t}
	(I)	(II)	(III)	(IV)	(V)	(VI)
D_t	0.364** (2.134)	0.297*** (3.164)	1.014*** (4.845)	-0.312* (-1.765)	-0.106 (-1.501)	-0.163 (-1.636)
$D_t \times y_{jt-1}$	0.125* (1.790)	0.227** (2.334)	-2.652*** (-4.873)	0.456*** (2.973)	-0.161 (-1.427)	-0.251 (-1.422)
$D_t \times y_{jt-2}$	0.194* (1.738)	0.246* (1.854)	0.462*** (4.845)	-0.175 (-1.648)	-0.175 (-1.477)	0.165 (1.457)
Others	control	control	control	control	control	control
F-statistic	4.676***	7.553***	11.620***	26.664***	23.812***	198.575***
$y_t : Awcc_{-s_t}$						
D_t	0.882** (2.416)	-0.546* (-1.747)	1.014*** (3.675)	-0.520 (-1.655)	-0.306*** (-2.699)	-0.379 (-1.443)
$D_t \times y_{jt-1}$	0.348* (1.755)	0.362** (2.312)	0.461** (2.133)	0.707*** (2.997)	0.260* (1.834)	-0.236 (-1.394)
$D_t \times y_{jt-2}$	0.253** (2.033)	0.211* (1.996)	0.161*** (3.676)	-0.145 (-1.487)	0.073 (1.112)	0.255 (1.476)
Others	control	control	control	control	control	control
F-statistic	10.657***	15.966***	14.626***	19.353***	110.073***	83.867***
$y_t : Avsn_{-s_t}$						
D_t	-0.082* (-1.780)	0.052** (2.174)	0.224** (2.421)	-0.185** (-2.226)	0.033* (1.810)	0.021 (1.565)
$D_t \times y_{jt-1}$	0.172** (2.182)	-0.091* (-1.943)	-0.288* (-1.938)	-0.383** (-2.527)	0.181 (1.310)	0.169 (1.493)
$D_t \times y_{jt-2}$	0.434** (2.118)	0.177** (2.018)	0.346*** (3.378)	-1.643*** (-4.657)	0.150 (1.237)	0.137 (1.461)
Others	control	control	control	control	control	control
F-statistic	5.181***	39.913***	6.729***	62.93***	15.627***	19.543***

y_{jt-2} are positive, with statistical significance observed at a minimum significance level of 10%. This demonstrates a structural breakpoint in the evolution of variable $Gden_t$ at the first policy changepoint. Examining columns (II) to (VI) of the first part of Table 7, we found that the coefficients of $D_t \times y_{jt-1}$ are significant at the 1% level in columns (II), (III) and (IV), but not significant in columns (V) and (VI). Meanwhile, the coefficient of D_t is significant at the 5% level in columns (III), (V) and (VI), and the coefficient of $D_t \times y_{jt-2}$ is only significant at the 10% level in column (II). These results suggest that the evolution of $Gden_t$

experiences slope changes at the first to fourth changepoints and jumps at the first, third, fifth, and sixth policy changepoints.

In the second part of Table 7, we observed that the evolution of variable $Awcc_t$ undergoes a significant change at the first, second, and third policy changepoints, and a jump occurs at the first and second policy changepoints. However, there are no significant breakpoints in the evolution process of $Awcc_t$ at the fourth, fifth, and sixth changepoints. Continuing to analyze the third part of Table 7, we found that $Avsn_t$ undergoes significant changes in evolution at policy changepoints

Table 9
Evolution trend of long-term EFRCN's global structural indicators near policy changepoints.

$y_t : Gden_I_t$	y_{1t}	y_{2t}	y_{3t}	y_{4t}	y_{5t}	y_{6t}
	(I)	(II)	(III)	(IV)	(V)	(VI)
D_t	-0.012 (-1.451)	-0.043 (-1.570)	-0.152 (-1.539)	0.138 (1.413)	0.051 (1.483)	-0.129 (-1.349)
$D_t \times y_{jt-1}$	-0.113 (-1.390)	-0.146 (-1.586)	0.437 (1.254)	-0.277 (-1.499)	0.186 (1.444)	-0.143 (-1.368)
$D_t \times y_{jt-2}$	-0.243 (-1.591)	0.260 (1.506)	-0.178* (-1.888)	-0.167 (-1.629)	-0.199 (-1.448)	-0.128 (-1.645)
Others	control	control	control	control	control	control
F-statistic	5.656***	6.204***	12.293***	12.945***	114.136***	28.044***
$y_t : Awcc_I_t$						
D_t	-0.005 (-1.636)	0.002* (1.831)	1.033** (2.106)	0.003 (1.432)	-0.036 (-1.249)	-0.003 (-1.457)
$D_t \times y_{jt-1}$	0.207 (1.414)	-0.224 (-1.635)	-0.219 (-1.305)	-0.184 (-1.631)	0.154 (1.123)	-0.161 (-1.315)
$D_t \times y_{jt-2}$	0.212 (1.164)	0.152 (1.465)	0.261 (1.281)	0.251 (1.449)	-0.118 (-1.308)	-0.125 (-1.564)
Others	control	control	control	control	control	control
F-statistic	3.669***	6.086***	5.792***	9.557***	155.828***	26.181***
$y_t : Avsn_I_t$						
D_t	0.045 (1.548)	-0.048 (-1.195)	0.176 (1.322)	0.019* (1.803)	-0.025 (-1.393)	-0.020 (-1.061)
$D_t \times y_{jt-1}$	0.221 (1.333)	0.193 (1.401)	-0.481 (-1.477)	0.347 (1.384)	-0.137 (-1.492)	-0.237 (-1.532)
$D_t \times y_{jt-2}$	0.132 (1.457)	0.243 (1.500)	-0.189 (-1.080)	0.211 (1.199)	0.247 (1.465)	-0.129 (-1.173)
Others	control	control	control	control	control	control
F-statistic	4.039***	7.552***	109.484***	9.274***	11.106***	93.371***

1, 2, 3, and 4, but not significant changes at changepoints 5 and 6. Summarizing the empirical results in Table 7, we found that the evolution process of non-periodic network structural indicators undergoes significant changes at policy changepoints 1, 2, and 3, while there are no significant changes at policy changepoints 5 and 6.

Table 8 reveals that for the short-term network, regression results of the global indicators $Gden_S_t$, $Awcc_S_t$, and $Avsn_S_t$ show at least one significant coefficient in the first to fourth columns at the 5% significance level, whereas most coefficients in columns (V) and (VI) are not significant. These results suggest that there is a significant change in the global structure of the short-term network at changepoints 1, 2, 3, and 4. Conversely, in Table 9, most coefficients are not significant, implying that there is no significant change in the global structure indicators of the long-term network at policy changepoints.

We could draw two main findings from the above empirical results. Firstly, the transition in lockdown policies has a significant impact on the non-periodic and short-term connectedness network structure of energy futures return, while the effect on the long-term network structure is insignificant. This indicates that the impact of policy transition on the connectedness of energy futures markets is primarily concentrated in the short-term. Secondly, the transitions in lockdown policies during the early stages (before June 2020) have a significant impact on the non-periodic and short-term network structure of the EFRCN, while the impact of policy changes during the middle and later stages on the structure of the EFRCN is not significant. One potential explanation for this result is the frequent occurrence of early policy changes, coupled with substantial and widespread adjustments in policy magnitude, which had a significant influence on the structure of the EFRCN.

5. Conclusions

Our analysis yields the following findings. Firstly, the rising population and GDP affected by the global COVID-19 pandemic-induced lockdown will increase the average density, average weighted clustering coefficient, and average strength of the EFRCN. This suggests that a heightened intensity of COVID-19 lockdown policies will reinforce the interdependence among energy futures markets. Secondly, in the non-periodic and short-term networks, an escalation in lockdown intensity

will increase the net spillover effects of oil and electricity futures while reducing those of natural gas and coal futures. However, in the long-term network, there is no significant decrease in the net spillover effects of coal futures as lockdown intensity increases. Thirdly, the structural shifts of COVID-19 lockdown policies mainly impact the non-periodic and short-term energy futures return connectedness network, whereas the impact on the long-term energy futures return connectedness network is not significant. Fourthly, the impact of the structural shifts of COVID-19 lockdown policies on the energy futures return connectedness network is primarily concentrated in the early stages of COVID-19 (before June 2020), and there are no significant changes in the network's structure during the later stages of the COVID-19 pandemic development.

This work provides us with the following implications. Implementing lockdown policies to curb the spread of epidemics enhances the level of connectedness among the returns of energy futures. This heightened connectedness increases the frequency of cross-market co-movements in energy futures markets, commonly known as "co-movement in ups and downs". The co-movement among energy futures markets can destabilize markets, thereby amplifying the risk associated with investing in energy futures markets. Hence, authorities that formulate intervention policies to control epidemic transmission should exercise caution when employing lockdown strategies. Utilizing lockdown measures necessitates considering their potential shocks on energy futures markets. Investors engaged in the energy futures market also ought to be attentive to the impact of lockdown strategies on the energy futures market. This is due to the fact that cross-market co-movements can attenuate the effectiveness of risk hedging for investment portfolios and augment both the potential gains and losses of the investment portfolios. For enterprises reliant on energy resources, a concern should also be directed towards the influence of lockdown policies on energy futures market prices. This pertains to the strong correlation between energy futures prices and spot prices, wherein alterations in energy futures prices can have an impact on spot prices.

Declaration of competing interest

The authors declare that they have no known competing financial

interests or personal relationships that could have appeared to influence the work reported in this article.

Data availability

Data will be made available on request.

Acknowledgments

This study has been supported by the National Natural Science Foundation of China (Grant Nos. 72273143 and 71974192) and the Interdisciplinary-Innovative Research Program of School of Interdisciplinary Studies, Renmin University of China.

Appendix A. Supplementary data

Supplementary data to this article can be found online at <https://doi.org/10.1016/j.jclepro.2023.139802>.

References

- Adams-Prassl, A., Boneva, T., Golin, M., Rauh, C., 2020. Inequality in the impact of the coronavirus shock: evidence from real time surveys. *J. Publ. Econ.* 189, 104245 <https://doi.org/10.1016/j.jpubeco.2020.104245>.
- Akyildirim, E., Cepni, O., Molnár, P., Uddin, G.S., 2022. Connectedness of energy markets around the world during the COVID-19 pandemic. *Energy Econ.* 109, 105900 <https://doi.org/10.1016/j.eneco.2022.105900>.
- Antonakakis, N., Chatziantoniou, I., Gabauer, D., 2020. Refined measures of dynamic connectedness based on time-varying parameter vector autoregressions. *J. Risk Financ. Manag.* 13, 84. <https://doi.org/10.3390/jrfm13040084>.
- Bahloul, S., Khemakhem, I., 2021. Dynamic return and volatility connectedness between commodities and Islamic stock market indices. *Resour. Policy* 71, 101993. <https://doi.org/10.1016/j.resourpol.2021.101993>.
- Barrat, A., Barthélemy, M., Pastor-Satorras, R., Vespignani, A., 2004. The architecture of complex weighted networks. *Proc. Natl. Acad. Sci. U. S. A.* 101, 3747–3752. <https://doi.org/10.1073/pnas.0400087101>.
- Bartik, A.W., Bertrand, M., Cullen, Z., Glaeser, E.L., Luca, M., Stanton, C., 2020. The impact of COVID-19 on small business outcomes and expectations. *Proc. Natl. Acad. Sci. U. S. A.* 117, 17656–17666. <https://doi.org/10.1073/pnas.2006991117>.
- Barunik, J., Krehlík, T., 2018. Measuring the frequency dynamics of financial connectedness and systemic risk. *J. Financ. Econ.* 16, 271–296. <https://doi.org/10.1093/jfinfec/nby001>.
- Behra, D.K., Sabreen, M., Sharma, D., 2021. The impact of COVID-19 on the Indian economy. *Int. Rev. Appl. Econ.* 35, 870–885. <https://doi.org/10.1080/02692171.2021.1962815>.
- Billio, M., Casarin, R., Costola, M., Iacopini, M., 2021. COVID-19 spreading in financial networks: a semiparametric matrix regression model. *Econom. Stat.* <https://doi.org/10.1016/j.ecosta.2021.10.003>.
- Boccalletti, S., Bianconi, G., Criado, R., del Genio, C.I., Gómez-Gardeñes, J., Romance, M., Sendiña-Nadal, I., Wang, Z., Zanin, M., 2014. The structure and dynamics of multilayer networks. *Phys. Rep.* 544, 1–122. <https://doi.org/10.1016/j.physrep.2014.07.001>.
- Bouri, E., Cepni, O., Gabauer, D., Gupta, R., 2021. Return connectedness across asset classes around the COVID-19 outbreak. *Int. Rev. Financ. Anal.* 73, 101646 <https://doi.org/10.1016/j.irfa.2020.101646>.
- Bouri, E., Naeem, M.A., Nor, S.M., Mbarki, I., Saeed, T., 2022. Government responses to COVID-19 and industry stock returns. *Econ. Res.-Ekon. Istraživanja* 35, 1967–1990. <https://doi.org/10.1080/1331677X.2021.1929374>.
- Chatziantoniou, I., Gabauer, D., Gupta, R., 2023. Integration and risk transmission in the market for crude oil: new evidence from a time-varying parameter frequency connectedness approach. *Resour. Policy* 84, 103729. <https://doi.org/10.1016/j.resourpol.2023.103729>.
- Chen, B., Li, J.S., Wu, X.F., Han, M.Y., Zeng, L., Li, Z., Chen, G.Q., 2018. Global energy flows embodied in international trade: a combination of environmentally extended input-output analysis and complex network analysis. *Appl. Energy* 210, 98–107. <https://doi.org/10.1016/j.apenergy.2017.10.113>.
- Chen, H., Xu, C., Peng, Y., 2022a. Time-frequency connectedness between energy and nonenergy commodity markets during COVID-19: evidence from China. *Resour. Policy* 78, 102874. <https://doi.org/10.1016/j.resourpol.2022.102874>.
- Chen, J., Wang, H., Zhong, R.Y., 2021. A supply chain disruption recovery strategy considering product change under COVID-19. *J. Manuf. Syst.* 60, 920–927. <https://doi.org/10.1016/j.jmsy.2021.04.004>.
- Chen, M., Qin, C., Zhang, X., 2022b. Cryptocurrency price discrepancies under uncertainty: evidence from COVID-19 and lockdown nexus. *J. Int. Money Finance* 124, 102633. <https://doi.org/10.1016/j.jimonfin.2022.102633>.
- Cheng, C., Barceló, J., Hartnett, A.S., Kubinec, R., Messerschmidt, L., 2020. COVID-19 government response event dataset (CoronaNet v1.0). *Nat. Human Behav.* 4, 756–768. <https://doi.org/10.1038/s41562-020-0909-7>.
- Clapp, J., Moseley, W.G., 2020. This food crisis is different: COVID-19 and the fragility of the neoliberal food security order. *J. Peasant Stud.* 47, 1393–1417. <https://doi.org/10.1080/03066150.2020.1823838>.
- Coccia, M., 2021. The relation between length of lockdown, numbers of infected people and deaths of Covid-19, and economic growth of countries: lessons learned to cope with future pandemics similar to Covid-19 and to constrain the deterioration of economic system. *Sci. Total Environ.* 775, 145801 <https://doi.org/10.1016/j.scitotenv.2021.145801>.
- Cui, J., Maghyereh, A., 2023. Higher-order moment risk connectedness and optimal investment strategies between international oil and commodity futures markets: insights from the COVID-19 pandemic and Russia-Ukraine conflict. *Int. Rev. Financ. Anal.* 86, 102520 <https://doi.org/10.1016/j.irfa.2023.102520>.
- Diebold, F.X., Yilmaz, K., 2012. Better to give than to receive: predictive directional measurement of volatility spillovers. *Int. J. Forecast.*, Special Sect. 1: Predictab. Financ. Markets 28, 57–66. <https://doi.org/10.1016/j.ijforecast.2011.02.006>.
- Diebold, F.X., Yilmaz, K., 2014. On the network topology of variance decompositions: measuring the connectedness of financial firms. *J. Econom., Causal, Predict., Specific. Anal.: Recent Adv. Fut. Direct.* 182, 119–134. <https://doi.org/10.1016/j.jeconom.2014.04.012>.
- Dong, Z., Li, Y., Zhuang, X., Wang, J., 2022. Impacts of COVID-19 on global stock sectors: evidence from time-varying connectedness and asymmetric nexus analysis. *North Am. J. Econ. Finance* 62, 101753. <https://doi.org/10.1016/j.najef.2022.101753>.
- Durbin, J., 1960. Estimation of parameters in time-series regression models. *J. R. Stat. Soc. Ser. B Methodol.* 22, 139–153. <https://doi.org/10.1111/j.2517-6161.1960.tb00361.x>.
- Farid, S., Naeem, M.A., Paltrinieri, A., Nepal, R., 2022. Impact of COVID-19 on the quantile connectedness between energy, metals and agriculture commodities. *Energy Econ.* 109, 105962 <https://doi.org/10.1016/j.eneco.2022.105962>.
- Fezzi, C., Fanghella, V., 2020. Real-time estimation of the short-run impact of COVID-19 on economic activity using electricity market data. *Environ. Resour. Econ.* 76, 885–900. <https://doi.org/10.1007/s10640-020-00467-4>.
- Forsythe, E., Kahn, L.B., Lange, F., Wiczer, D., 2020. Labor demand in the time of COVID-19: evidence from vacancy postings and UI claims. *J. Publ. Econ.* 189, 104238 <https://doi.org/10.1016/j.jpubeco.2020.104238>.
- González, M. de la, Jareño, F., Skinner, F.S., 2021. Asymmetric interdependencies between large capital cryptocurrency and Gold returns during the COVID-19 pandemic crisis. *Int. Rev. Financ. Anal.* 76, 101773 <https://doi.org/10.1016/j.irfa.2021.101773>.
- Goolsbee, A., Syverson, C., 2021. Fear, lockdown, and diversion: comparing drivers of pandemic economic decline 2020. *J. Publ. Econ.* 193, 104311 <https://doi.org/10.1016/j.jpubeco.2020.104311>.
- Guzmán, A., Pinto-Gutiérrez, C., Trujillo, M.-A., 2021. Trading cryptocurrencies as a pandemic pastime: covid-19 lockdowns and bitcoin volume. *Mathematics* 9. <https://doi.org/10.3390/math9151771>.
- Hale, T., Angrist, N., Goldszmidt, R., Kira, B., Petherick, A., Phillips, T., Webster, S., Cameron-Blake, E., Hallas, L., Majumdar, S., Tatlow, H., 2021. A global panel database of pandemic policies (Oxford COVID-19 Government Response Tracker). *Nat. Human Behav.* 5, 529–538. <https://doi.org/10.1038/s41562-021-01079-8>.
- Huang, J., Chen, B., Xu, Y., Xia, X., 2023. Time-frequency volatility transmission among energy commodities and financial markets during the COVID-19 pandemic: a Novel TVP-VAR frequency connectedness approach. *Finance Res. Lett.* 53 <https://doi.org/10.1016/j.frl.2023.103634>.
- Katsiampa, P., Yarovaya, L., Zięba, D., 2022. High-frequency connectedness between Bitcoin and other top-traded crypto assets during the COVID-19 crisis. *J. Int. Financ. Mark. Inst. Money* 79, 101578. <https://doi.org/10.1016/j.intfin.2022.101578>.
- Ke, X., Hsiao, C., 2022. Economic impact of the most drastic lockdown during COVID-19 pandemic—the experience of Hubei, China. *J. Appl. Econom.* 37, 187–209. <https://doi.org/10.1002/jae.2871>.
- Killick, R., Fearnhead, P., Eckley, I.A., 2012. Optimal detection of changepoints with a linear computational cost. *J. Am. Stat. Assoc.* 107, 1590–1598. <https://doi.org/10.1080/01621459.2012.737745>.
- Kivela, M., Arenas, A., Barthélemy, M., Gleeson, J.P., Moreno, Y., Porter, M.A., 2014. Multilayer networks. *J. Complex Netw.* 2, 203–271. <https://doi.org/10.1093/comnet/cnu016>.
- Koop, G., Korobilis, D., 2014. A new index of financial conditions. *Eur. Econ. Rev.* 71, 101–116. <https://doi.org/10.1016/j.euroeconrev.2014.07.002>.
- Liu, J., 2023. Time-frequency correlations and extreme spillover effects between carbon markets and NFTs: the roles of EPU and COVID-19. *Finance Res. Lett.* 54, 103690 <https://doi.org/10.1016/j.frl.2023.103690>.
- Liu, P., Huang, W.-Q., 2022. Modelling international sovereign risk information spillovers: a multilayer network approach. *North Am. J. Econ. Finance* 63, 101794. <https://doi.org/10.1016/j.najef.2022.101794>.
- McKibbin, W., Fernando, R., 2021. The global macroeconomic impacts of covid-19: seven scenarios. *Asian Econ. Pap.* 20, 2–30. https://doi.org/10.1162/asep_a_00796.
- Mensi, W., Vo, X.V., Kang, S.H., 2023. Quantile spillovers and connectedness analysis between oil and African stock markets. *Econ. Anal. Pol.* 78, 60–83. <https://doi.org/10.1016/j.eap.2023.02.002>.
- Mishra, A.K., Arunachalam, V., Olson, D., Patnaik, D., 2023. Dynamic connectedness in commodity futures markets during Covid-19 in India: new evidence from a TVP-VAR extended joint connectedness approach. *Resour. Policy* 82, 103490. <https://doi.org/10.1016/j.resourpol.2023.103490>.
- Ouyang, R., Zhuang, C., Wang, T., Zhang, X., 2022. Network analysis of risk transmission among energy futures: an industrial chain perspective. *Energy Econ.* 107, 105798 <https://doi.org/10.1016/j.eneco.2021.105798>.
- Pedreschi, N., Battaglia, D., Barrat, A., 2022. The temporal rich club phenomenon. *Nat. Phys.* 18, 931–938. <https://doi.org/10.1038/s41567-022-01634-8>.

- Qi, H., Wu, T., Chen, H., Lu, X., 2023. Time-frequency connectedness and cross-quantile dependence between carbon emission trading and commodity markets: evidence from China. *Resour. Policy* 82, 103418. <https://doi.org/10.1016/j.resourpol.2023.103418>.
- Restrepo, N., Uribe, J.M., Manotas, D., 2018. Financial risk network architecture of energy firms. *Appl. Energy* 215, 630–642. <https://doi.org/10.1016/j.apenergy.2018.02.060>.
- Ruiz Sánchez, G., 2021. Monthly suicide rates during the COVID-19 pandemic: evidence from Japan. *Econ. Lett.* 207, 110014 <https://doi.org/10.1016/j.econlet.2021.110014>.
- Shehzad, K., Bilgili, F., Zaman, U., Kocak, E., Kuskaya, S., 2021. Is gold favourable than bitcoin during the COVID-19 outbreak? Comparative analysis through wavelet approach. *Resour. Policy* 73, 102163. <https://doi.org/10.1016/j.resourpol.2021.102163>.
- Shehzad, K., Xiaoxing, L., Kazouz, H., 2020. COVID-19's disasters are perilous than Global Financial Crisis: a rumor or fact? *Finance Res. Lett.* 36, 101669 <https://doi.org/10.1016/j.frl.2020.101669>.
- So, M.K.P., Chan, L.S.H., Chu, A.M.Y., 2021a. Financial network connectedness and systemic risk during the COVID-19 pandemic. *Asia Pac. Financ. Mark.* 28, 649–665. <https://doi.org/10.1007/s10690-021-09340-w>.
- So, M.K.P., Chu, A.M.Y., Chan, T.W.C., 2021b. Impacts of the COVID-19 pandemic on financial market connectedness. *Finance Res. Lett.* 38, 101864 <https://doi.org/10.1016/j.frl.2020.101864>.
- Tchouamou Njoya, E., 2023. Assessing the poverty impact of the COVID-19-induced tourism crisis in Tanzania: a social accounting matrix microsimulation analysis. *J. Sustain. Tourism* 31, 801–820. <https://doi.org/10.1080/09669582.2021.2024552>.
- Truong, C., Oudre, L., Vayatis, N., 2020. Selective review of offline change point detection methods. *Signal Process.* 167, 107299 <https://doi.org/10.1016/j.sigpro.2019.107299>.
- Umar, Z., Gubareva, M., 2020. A time–frequency analysis of the impact of the Covid-19 induced panic on the volatility of currency and cryptocurrency markets. *J. Behav. Exp. Finance* 28, 100404. <https://doi.org/10.1016/j.jbef.2020.100404>.
- Wang, Q., Cao, S., Xiao, Y., 2019. Statistical characteristics of international conflict and cooperation network. *Phys. Stat. Mech. Appl.* 535, 122334 <https://doi.org/10.1016/j.physa.2019.122334>.
- Wu, J., Zhan, X., Xu, H., Ma, C., 2023. The economic impacts of COVID-19 and city lockdown: early evidence from China. *Struct. Change Econ. Dynam.* 65, 151–165. <https://doi.org/10.1016/j.strueco.2023.02.018>.
- Wu, X., Nazari, N., Griffiths, M.D., 2021. Using fear and anxiety related to covid-19 to predict cyberchondria: cross-sectional survey study. *J. Med. Internet Res.* 23 <https://doi.org/10.2196/26285>.